**Article**

# Assessment of long-term particulate nitrate air pollution and its health risk in China



2018 Population Weighted NO₃-

2018 Death Rate of NO₃- Pollution

Yun Hang, Xia Meng, Tiantian Li, ..., Haidong Kan, Xiaoming Shi, Yang Liu

shixm@chinacdc.cn (X.S.)
yang.liu@emory.edu (Y.L.)

**Highlights**

We build a $NO_3^-$ model using machine learning techniques incorporating satellite data

We estimate spatiotemporal variations of $NO_3^-$ concentration in China from 2005–2018

In 2018, the national mean mortality burden attributable to $NO_3^-$ was about 0.68 million

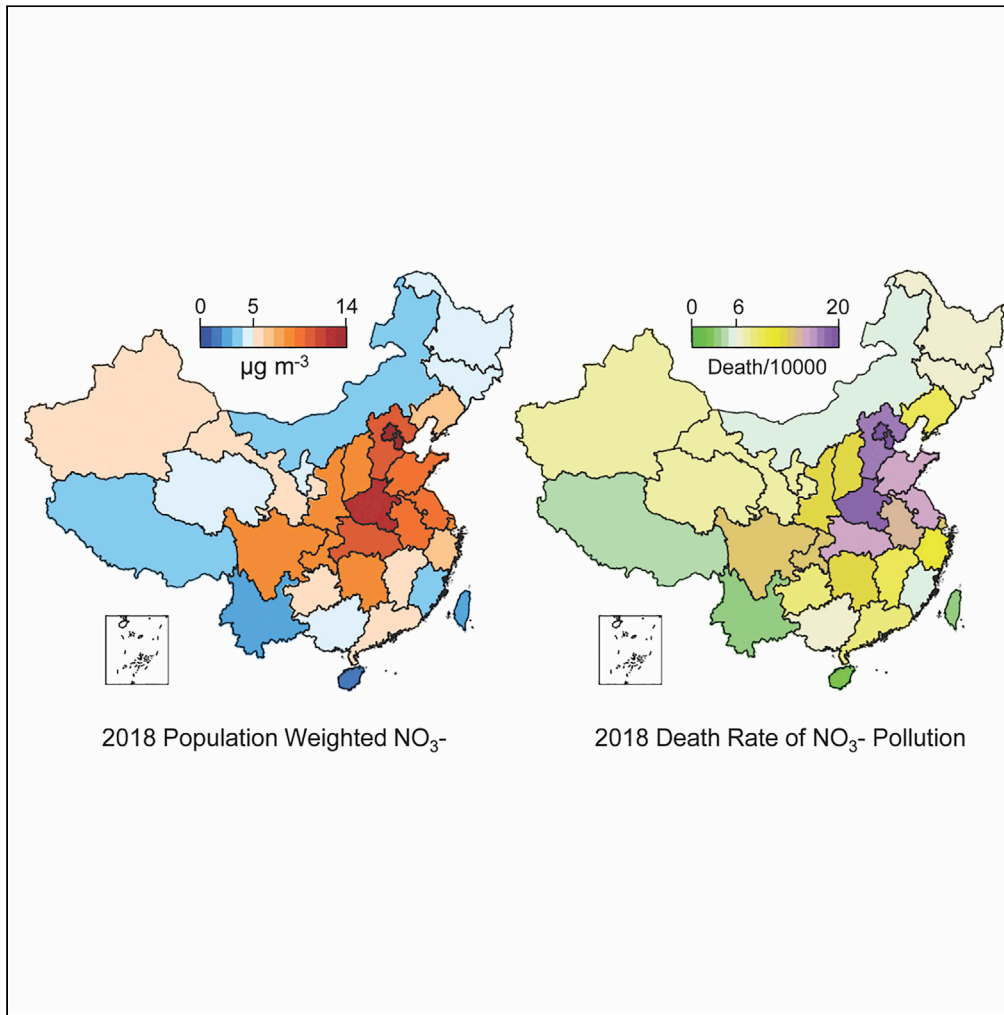Targeted regulations on vehicle emissions are needed to control $NO_3^-$ pollution in China

## Article

# Assessment of long-term particulate nitrate air pollution and its health risk in China

Yun Hang,[1,11] Xia Meng,[2,11] Tiantian Li,[3] Tijian Wang,[4] Junji Cao,[5] Qingyan Fu,[6] Sagnik Dey,[7] Shenshen Li,[8] Kan Huang,[9] Fengchao Liang,[10] Haidong Kan,[2] Xiaoming Shi,[3,*] and Yang Liu[1,12,*]

## SUMMARY

**Air pollution is a major environmental and public health challenge in China and the Chinese government has implemented a series of strict air quality policies. However, particulate nitrate ($NO_3^-$) concentration remains high or even increases at monitoring sites despite the total $PM_{2.5}$ concentration has decreased. Unfortunately, it has been difficult to estimate $NO_3^-$ concentration across China due to the lack of a $PM_{2.5}$ speciation monitoring network. Here, we use a machine learning model incorporating ground measurements and satellite data to characterize the spatiotemporal patterns of $NO_3^-$, thereby understanding the disease burden associated with long-term $NO_3^-$ exposure in China. Our results show that existing air pollution control policies are effective, but increased $NO_3^-$ of traffic emissions offset reduced $NO_3^-$ of industrial emissions. In 2018, the national mean mortality burden attributable to $NO_3^-$ was as high as 0.68 million, indicating that targeted regulations are needed to control $NO_3^-$ pollution in China.**

## INTRODUCTION

Ambient fine particulate matter ($PM_{2.5}$, or particulate matter with an aerodynamic diameter of less than 2.5 μm) pollution has been identified as a leading environmental risk factor for premature death worldwide (Cohen et al., 2017; Burnett et al., 2018). For example, long-term $PM_{2.5}$ exposures in China are estimated to account for 30.8 million adult premature deaths during 2000–2016 (Liang et al., 2020). In response to improving air quality, the Chinese government has promulgated a series of strict clean air policies and effectively reduced $PM_{2.5}$ pollution (Xiao et al., 2018). However, $PM_{2.5}$ is a complex mixture of many constituents such as sulfate ($SO_4^-$), nitrate ($NO_3^-$), organic carbon, elemental carbon, mineral dust, and sea salt. Previous studies suggested that various $PM_{2.5}$ components may pose different adverse effects on human health (WHO, 2007; Park et al., 2018). Numerous population-based epidemiological studies have provided evidence that long-term and short-term exposures to $NO_3^-$ are associated with increased risks of mortality, hospital admissions, emergency department visits of cardiovascular diseases, respiratory diseases, and total non-accidental diseases (Peng et al., 2009; Ostro et al., 2009, 2015; Cao et al., 2012; Son et al., 2012; Liu and Zhang, 2015; Chung et al., 2015; Lin et al., 2016). In addition, recent studies based on human cell lines and mouse experiments have found that water-soluble inorganics of particulate matters including $NO_3^-$ could rapidly penetrate the lung surfactant barrier to the alveolar region and perturb gene expression in the lungs, as well as resulting in lung injuries and metabolite changes in serum samples of mice (Zhao et al., 2019).

There is an urgent need to estimate $NO_3^-$ in China and quantify the mortality burden associated with its long-term exposures. In recent years, $NO_3^-$ is becoming the dominant component of $PM_{2.5}$ during haze events in China (Xu et al., 2019; Feng et al., 2021; Shao et al., 2018; Kong et al., 2020) despite $NO_3^-$ precursor, $NO_X$ ($NO_2 + NO$), has decreased by about 20% under proactive policies (Zheng et al., 2018). This is due to the fact that $NO_3^-$ formation is not only affected by $NO_X$ but also the availability of $SO_4^-$ precursor, $SO_2$, since $NO_3^-$ and $SO_4^-$ are closely connected by the participation of bases (mainly ammonia, $NH_3$) (Stelson et al., 1984). $SO_2$ has dropped by 62% from 2010 to 2017 because desulphurization is one of China's major air pollution control policies (Zheng et al., 2018). Before the major reduction of $SO_2$, $NH_3$ neutralized $SO_2$ first because ammonium sulfate (($NH_4$)$_2SO_4$) has better stability than ammonium nitrate ($NH_4NO_3$) (Liu et al., 2012). After the reduction, more free $NH_3$ becomes available to form $NH_4NO_3$ and increases $NO_3^-$ formation yields. Another possible explanation for the increasing $NO_3^-$ is that urban $NH_3$ sources

[1]Gangarosa Department of Environmental Health, Rollins School of Public Health, Emory University, Atlanta, GA 30322, USA

[2]School of Public Health, Fudan University, Shanghai 200032, China

[3]China CDC Key Laboratory of Environment and Population Health, National Institute of Environmental Health, Chinese Center for Disease Control and Prevention, Beijing 100021, China

[4]School of Atmospheric Sciences, Nanjing University, Nanjing 210023, China

[5]Institute of Atmospheric Physics (IAP), Chinese Academy of Sciences, Beijing 100101, China

[6]State Ecologic Environmental Scientific Observation and Research Station at Dianshan Lake, Shanghai Environmental Monitoring Center, Shanghai 200235, China

[7]Centre for Atmospheric Sciences, Indian Institute of Technology Delhi, Hauz Khas, New Delhi 110016, India

[8]State Key Laboratory of Remote Sensing Science, Aerospace Information Research Institute (AIR), Chinese Academy of Sciences, Beijing 100101, China

[9]Shanghai Key Laboratory of Atmospheric Particle Pollution and Prevention (LAP3), Department of Environmental Science and Engineering, Fudan University, Shanghai 200433, China

[10]School of Public Health and Emergency Management, Southern University of Science and Technology, Shenzhen 518055, China

[11]These authors contributed equally

[12]Lead contact

*Continued*

from vehicle emissions are expanding due to the rapidly growing domestic vehicle fleet (Liu et al., 2013; Chang et al., 2016; Sun et al., 2017). As reported by the National Bureau of Statistics of China, the civilian vehicle population increased from 31.6 million in 2005 to 232.3 million in 2018 (Figure S1).

Although $NO_3^-$ is of elevated toxicity and its fraction in $PM_{2.5}$ is growing, the health impact of long-term $NO_3^-$ pollution in China has not been investigated due to the lack of accurate exposure estimates. To date, only a few studies utilized chemical transport models (CTMs) predicted China's $NO_3^-$ concentration at the national level (Xing et al., 2015; Geng et al., 2019; Zhai et al., 2021; Liu et al., 2017a). However, the performance of CTMs heavily relies on emission inventories, which usually bring large uncertainties in developing countries where emission information is inaccurate (Li et al., 2017). Recently, a prediction model was built based on the GEOS-Chem atmospheric chemistry model to simulate seasonal $NO_3^-$ concentration in China from 2013–2018 with a correlation coefficient (r) value of 0.82 in winter (Zhai et al., 2021). This $NO_3^-$ model can provide predictions in large-scale geographical zones such as North China but is limited in providing information on $NO_3^-$ over smaller regions (i.e., cities and roads) limited by its coarse resolution of 0.5 × 0.625°. However, the concentration field at finer resolution is important for identifying anthropogenic drivers of changes in $NO_3^-$. For example, it is necessary to estimate $NO_3^-$ along major traffic corridors because $NO_3^-$ formation is likely associated with expanding vehicle emissions (Fan et al., 2020). In addition, the model cannot predict $NO_3^-$ over Northwest China, where the source of air pollution is gradually shifting from natural dust storms to anthropogenic industrial emissions (Turap et al., 2019). Moreover, the model only predicts $NO_3^-$ after implementing APPCAP in 2013, thereby failing to evaluate the effectiveness of early air quality regulations, including those related to fuel quality standards. Therefore, a national-wide, high-resolution, long-term prediction model is required to estimate the spatiotemporal patterns of $NO_3^-$ for policy assessment and advance the effort on understanding the mortality burden associated with long-term $NO_3^-$ exposures in China.

Assessing the trend of historical air pollution across China without a ground monitoring network is challenging. Machine learning models that incorporate ground measurements, satellite remote sensing data, and other supporting information are one of the emerging solutions (Xiao et al., 2018). We employed a random forest algorithm (Breiman, 2001), a machine learning model, driven by satellite-retrieved aerosol data to build a $NO_3^-$ prediction model. The out-of-bag (OOB) bootstrap sampling strategy of the random forest algorithm was used to develop and validate the model (Meng et al., 2018b). This method allows a flexible number of predictors to estimate relationships between $NO_3^-$ and various impact factors such as the spatial distribution of road length, which is closely related to $NO_3^-$ concentration but is not incorporated in previously published $NO_3^-$ models (Xing et al., 2015; Geng et al., 2019; Zhai et al., 2021; Liu et al., 2017a; Li et al., 2021). Specifically, we incorporated aerosol optical depth (AOD), a measure of the amount of aerosol present in the atmosphere, retrieved by the Multi-angle Imaging SpectroRadiometer (MISR) onboard Terra satellite to provide unique information on $PM_{2.5}$ constituents over land (Kahn et al., 2005; Chau et al., 2020). Compared with existing $NO_3^-$ models that only involved ground observations from several monitoring sites over short periods, we collected daily mean $NO_3^-$ concentration from 88 urban and rural monitoring sites across China from 2005–2018, including high-quality measurements from Hong Kong and Taiwan $PM_{2.5}$ speciation supersites (Lin et al., 2008; Huang et al., 2014). Detailed information on ground $NO_3^-$ observations used in model development is provided in Table S1.

Here, we applied the newly developed $NO_3^-$ model to address the following research questions: (1) What is the temporal trend of $NO_3^-$ concentration in China from 2005–2018? (2) What are the long-term spatial variations in the $NO_3^-$ concentration? And (3) How large is the mortality burden due to the $NO_3^-$ exposure? We compared the trend of $NO_3^-$ over four city clusters in China, including Beijing–Tianjin–Hebei (BTH), the biggest urbanized megalopolis in North China with a population of 110 million in 2020; Yangtze River Delta (YRD), the fastest growing and the most developed region in East China; Pearl River Delta (PRD), the most densely urbanized region in South China; and Cheng-Yu (CY), the fourth powerhouse that drives China's economic growth. We then estimated the spatial and temporal characteristics of all-cause excess mortality attributable to $NO_3^-$ exposure in China based on published analyses. The detailed methodology is provided in the STAR Methods section.

## RESULTS AND DISCUSSION
### High-performance $NO_3^-$ concentration model
Our study domain covers mainland China, Taiwan, Hong Kong, and Macao, as demonstrated in Figure 1. The circles represent the location of monitoring sites color-coded by daily mean $NO_3^-$ concentration. In

*Correspondence:
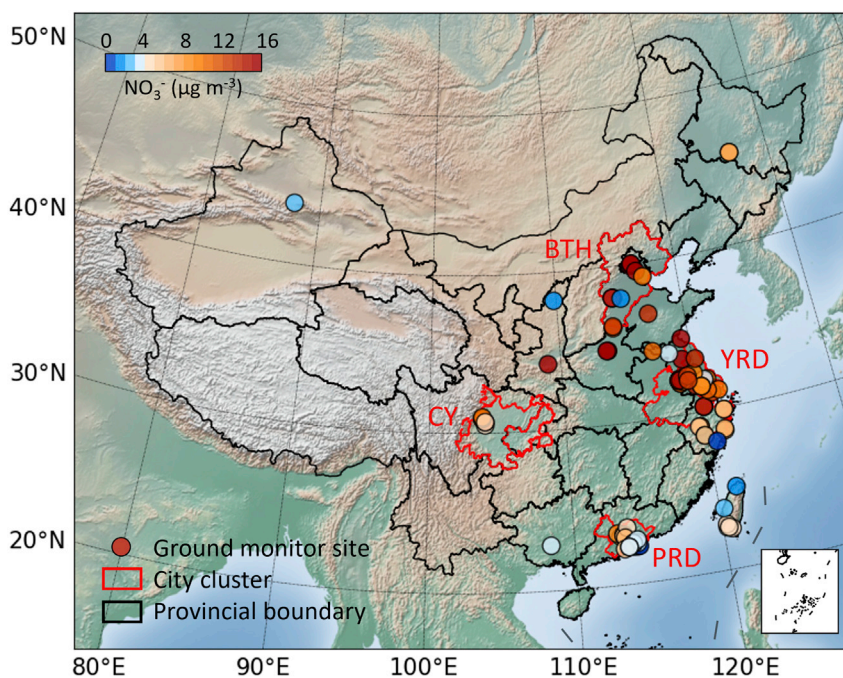shixm@chinacdc.cn (X.S.),
yang.liu@emory.edu (Y.L.)

**Figure 1. Map of study domain, the spatial distribution of ground monitoring sites, and averaged daily mean NO₃₋ concentrations from 2005–2018.**

The circles show the location of ground monitoring sites for measuring $NO_3^-$ concentrations. The color of these circles represents the value of the calculated daily mean $NO_3^-$ concentration with a color bar located at the top left corner. Four city clusters (i.e., Beijing–Tianjin–Hebei (BTH), Yangtze River Delta (YRD), Pearl River Delta (PRD), Cheng-Yu (CY)), and provinces of China are labeled by red and black lines, respectively.

general, $NO_3^-$ was high in populous city clusters. Taking the BTH region as an example, Beijing's daily mean $NO_3^-$ concentration was about 16 $\mu g\,m^{-3}$, which was more than four times higher than that of developed countries (Ostro et al., 2015), indicating estimating $NO_3^-$ in China is urgently needed. Using ground observations to train a random forest model driven by satellite data and other supporting information, we developed a high-performance model to predict daily $NO_3^-$ concentration in China at 10-km resolution. Specifically, this model considered atmospheric compositions (i.e., $NO_2$), meteorological conditions (i.e., temperature), emission inventories (i.e., $NH_3$), vegetation cover (i.e., Normalized Difference Vegetation Index, NDVI), and road length (Figure S2). MISR AOD data that is unique in characterizing the shape, size, and light-absorbing property of $PM_{2.5}$ constituents were incorporated to help identify complicated spatiotemporal variance of $NO_3^-$, which CTMs can simulate but with large uncertainties (Xing et al., 2015; Geng et al., 2019, 2020; Friberg et al., 2016; Liu et al., 2007; Franklin et al., 2017; Meng et al., 2018a).

Figure S3 shows that model-calculated monthly mean $NO_3^-$ concentrations are in good agreement with observations collected from monitoring sites as the slope of regression lines is close to unity with intercepts close to zero. The model's OOB cross-validation (CV) $R^2$ value is 0.88 (Figure S3A), indicating little prediction bias. We conducted spatial and temporal CVs to test whether the model could make reliable predictions where or when ground observations were unavailable (Figures S3B and S3C). In the spatial CV test, ground $NO_3^-$ observations were divided into groups based on the monitoring site location. $NO_3^-$ predictions were generated by a random forest model trained with data elsewhere. Similarly, the temporal CV was tested with data divided by the time when ground $NO_3^-$ was measured.

Figure 2 displays time-series comparisons between predicted and measured monthly mean $NO_3^-$ concentrations in six geographical regions in China. Only a few monitoring sites documented $NO_3^-$ before 2013, such as the one in Xi'an, located in Northwest China. $NO_3^-$ level of Xi'an was high in winter and low in summer (red line in Figure 2A). Our model successfully predicts this seasonal cycle and extreme values (black line in Figure 2A). Compared with high-quality observations in Taiwan supersites, our model accurately simulates the decreasing trend of $NO_3^-$ in Pingtung (Figure 2B). Starting from 2013, ground monitoring sites of
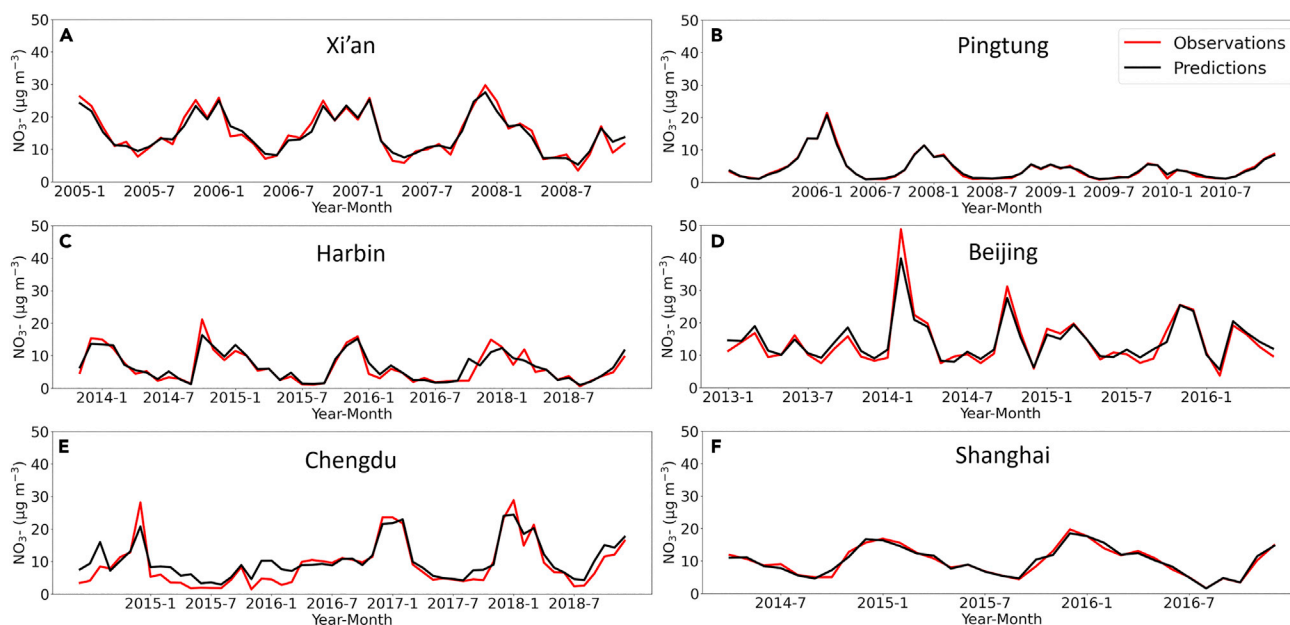
**Figure 2. Predicted and observed monthly mean NO₃⁻ concentrations at six monitoring sites of different geographical regions in China.**
In each figure, the red line represents monthly mean NO₃⁻ observations while model-calculated NO₃⁻ predictions are shown as the black line. Two sites are selected to display NO₃⁻ levels over 2005–2012 (pre APPCAP), including the site located at (A) Xi'an in the Northwest and (B) Pingtung in the South. (C)–(F) show results from 2013–2018 (during APPCAP) of sites located at (C) Harbin in the Northeast, (D) Beijing in the North, (E) Chengdu in the West, and (F) Shanghai in the East.

NO₃⁻ have become available in many other regions in China. We present the comparison result of four sites, including Harbin in the Northeast, Beijing in the North, Chengdu in the West, and Shanghai in the East (Figures 2C–2F). We find that Beijing is the only city where NO₃⁻ concentration has decreased since the implementation of APPCAP (Figure 2D). The NO₃⁻ level was stable in Harbin and Shanghai after 2014 (Figures 2C and 2F). In Chengdu, NO₃⁻ concentration even increased to 30 μg m⁻³ in January 2018 (Figure 2E), which doubled the WHO's standard on 24-h total PM₂.₅ (15 μg m⁻³), suggesting reducing NO₃⁻ is crucially important for promoting public health in China. Interestingly, NO₃⁻ was unusually low in Chengdu in winter 2016, likely related to abnormal meteorological conditions (Zhai et al., 2021; Zhang et al., 2019b; Zhou et al., 2019). Overall, Figure 2 indicates that our model has the potential to accurately predict monthly NO₃⁻ concentration over different geographical regions. Compared with recent studies predicting NO₃⁻ in China (Zhai et al., 2021; Li et al., 2021), our model exhibits higher accuracy with a longer temporal and broader spatial coverage.

### Temporal trend of NO₃⁻ concentration from 2005–2018

Based on the newly developed NO₃⁻ model, we estimated the temporal trend of China's national annual mean NO₃⁻ concentration as depicted in the red line of Figure 3. The linear trend of NO₃⁻ was calculated over two periods, 2005–2012 (pre APPCAP) and 2013–2018 (during APPCAP), shown as gray lines in Figure 3. During the pre APPCAP, the national mean NO₃⁻ concentration peaked at 9.2 μg m⁻³ in 2006 and decreased to 8.4 μg m⁻³ in 2012. This reduction was likely due to the Chinese government releasing the 11th Five Year Plan (2006–2011), effectively reducing emissions from industrial facilities (Jin et al., 2016). In addition, two vehicle NOₓ emission standards were established, including National III released in 2007 and National IV released in 2011, to control on-road vehicle emissions (Wu et al., 2017). During APPCAP, the national mean NO₃⁻ slightly decreased from 9.3 μg m⁻³ to 7.6 μg m⁻³ with a linear trend of −0.3 μg m⁻³ from 2013–2018. The decreasing trend was contributed by the 12th Five Year Plan (2012–2017), and APPCAP promoted accelerating denitrification and required all coal-fired units except circulating fluidized bed boilers to install denitrification facilities (2013). However, the rapidly growing vehicle population (Figure S1) increased NO₃⁻ generated from traffic emissions, offsetting reduced NO₃⁻ from industrial emissions (Fan et al., 2020). Moreover, the rate of the decreasing NO₃⁻ from coal combustions slowed down gradually due to mitigation actions were the most effective at an early stage (Zhong et al., 2021). The minimum national mean NO₃⁻ appeared in 2016 at 7.4 μg m⁻³ was likely influenced by favorable
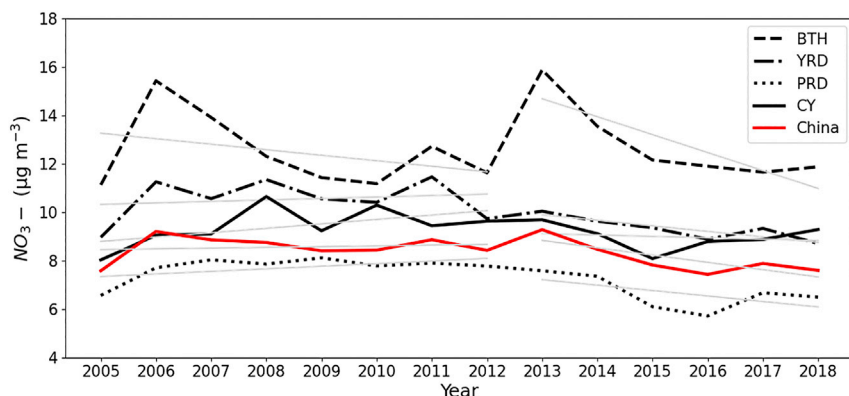
**Figure 3. Annual mean NO₃- concentrations of China and four city clusters during 2005–2018.**
The trends are calculated based on the newly developed $NO_3^-$ prediction model. The red line shows the estimated national annual mean $NO_3^-$ concentrations. The four black lines represent the population-weighted annual mean $NO_3^-$ concentrations of four city clusters. The gray lines are calculated linear trends over 2005–2012 (pre APPCAP) and 2013–2018 (during APPCAP).

meteorological conditions that suppressed $NO_3^-$ formation (Zhang et al., 2019b). Compared to other $PM_{2.5}$ constituents like $SO_4^-$, $NO_3^-$ is much more sensitive to temperature. For example, thermodynamic formation of $NH_4NO_3$ favors low temperatures (Zhai et al., 2021; Zhou et al., 2019). Winter 2016 was much warmer than normal (Zhang et al., 2019b), which may contribute to the low $NO_3^-$ level. Overall, the national mean $NO_3^-$ was relatively stable with a range of less than $2\ \mu g\ m^{-3}$ during the whole study period and even slightly increased in recent years, which is consistent with findings of existing studies (Zhai et al., 2021; Zhao et al., 2022).

To understand the temporal variation of $NO_3^-$ across different populated regions, we calculated the annual mean population-weighted $NO_3^-$ of four major city clusters (BTH, YRD, PRD, and CY) shown as black lines in Figure 3. BTH (dashed line) was the most polluted cluster during the entire study period as BTH had not only numerous coal-fired power plants but also a large number of vehicles, which are major sources of generating $NO_x$ (Zhao et al., 2012). The annual mean $NO_3^-$ of BTH ranged from $11.1$–$15.4\ \mu g\ m^{-3}$ with a linear trend of $-0.23\ \mu g\ m^{-3}$ before implementing APPCAP. Note that BTH is the only cluster with a decreasing $NO_3^-$ trend, contributed by strict air control policies during Beijing Olympic Games and local vehicle regulations (Chen et al., 2013; van der A et al., 2017). For example, a ban on high emission cars was enforced in Beijing but not nationwide. During APPCAP, the $NO_3^-$ level of BTH substantially decreased from $15.9\ \mu g\ m^{-3}$ in 2013 to $12.2\ \mu g\ m^{-3}$ in 2015, but became stable with a range of $11.7$–$11.9\ \mu g\ m^{-3}$ after 2015, dominating the temporal trend of the national $NO_3^-$ level (red line). This tendency was most likely influenced by a significant increase in traffic emissions (Fan et al., 2020). Also, BTH had extensive agricultural activities that provided abundant $NH_3$ to form $NO_3^-$, especially when $SO_2$ emission reductions significantly increased over the BTH after 2013 (Liu et al., 2018). The $NO_3^-$ level of YRD and CY clusters was similar, ranging from $8.0$–$11.3\ \mu g\ m^{-3}$ during the study period with increasing trends ($+0.06\ \mu g\ m^{-3}$ and $+0.18\ \mu g\ m^{-3}$) from 2005–2012, and slightly decreasing trends ($-0.23\ \mu g\ m^{-3}$ and $-0.06\ \mu g\ m^{-3}$) from 2013–2018 despite APPCAP set ambitious goals in these clusters (Zhang et al., 2019a). The lowest $NO_3^-$ level was found in PRD where climate temperature is much higher than the other three clusters that may relatively restrain $NO_3^-$ formation (Zhai et al., 2021; Zhou et al., 2019). The trend of $NO_3^-$ in PRD changed from $+0.11\ \mu g\ m^{-3}$ (pre APPCAP) to $-0.22\ \mu g\ m^{-3}$ (during APPCAP), with $NO_3^-$ concentration ranging between $5.7$ and $8.1\ \mu g\ m^{-3}$.

**Long-term spatial variations in $NO_3^-$ concentration**

The spatial distribution of annual mean $NO_3^-$ concentration in China during 2005–2018 is mapped in Figure 4. Interestingly, the general spatial distribution of $NO_3^-$ is similar to the distribution of estimated agricultural $NH_3$ emissions in China (Zhang et al., 2018), showing that regulation of $NH_3$ is an important component of $NO_3^-$ reduction (Wu et al., 2016). In addition, high $NO_3^-$ concentration (colored in red) occurred over three types of regions. First, $NO_3^-$ was especially high along major transportation corridors such as national highways of China, which has not been reported in previous studies (Xing et al., 2015; Geng et al., 2017, 2019; Zhai et al., 2021; Li et al., 2021). For example, the level of $NO_3^-$ in BTH generally ranged
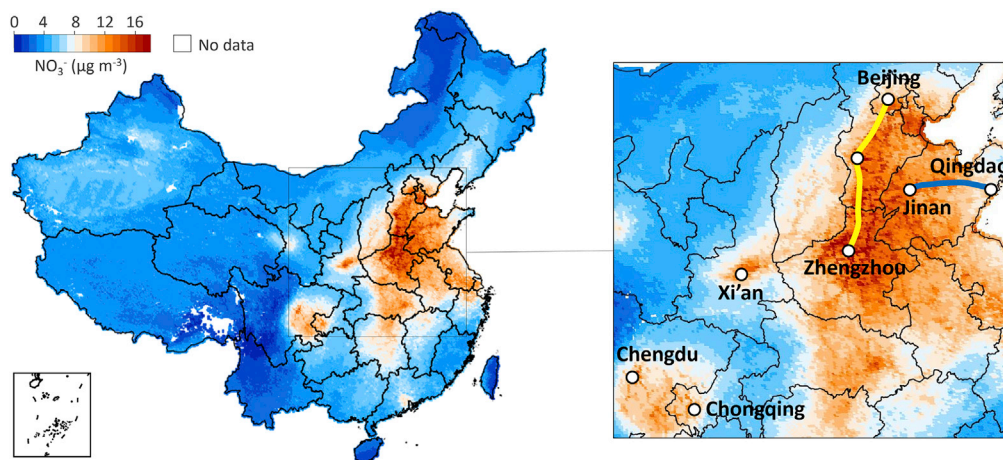
**Figure 4. Spatial distribution of annual mean NO₃- concentrations in China, 2005–2018.**
The thick lines in the right-side figure refer to the section of G4 Beijing-Hong Kong and Macau Expressway (yellow) and G20 Qingdao-Yinchuan Expressway (blue).

from 5 to 10 $\mu g\,m^{-3}$ but increased by more than twice over the upper section of G4 Beijing-Hong Kong and Macau Expressway (thick yellow line). In Shandong province, $NO_3^-$ rose to 15 $\mu g\,m^{-3}$ along G20 Qingdao-Yinchuan Expressway (thick blue line) while the background $NO_3^-$ was about 10 $\mu g\,m^{-3}$. Similarly, $NO_3^-$ was higher than 15 $\mu g\,m^{-3}$ over cities with dense road networks (i.e., Xi'an, Zhengzhou) or large vehicle populations (i.e., Chengdu and Chongqing). These elevated $NO_3^-$ levels suggest that control of vehicle emissions would be the key to reducing $NO_3^-$ pollution in China (Fan et al., 2020).

Second, $NO_3^-$ pollution was severe in areas with many coal combustions and extensive industry facilities (i.e., Shandong and Henan). Taking Shandong as an example, a province in North China where coal burning is commonly used for household heating (Shen et al., 2020), $NO_3^-$ was always above 10 $\mu g\,m^{-3}$. It was estimated that 67% of $NO_x$ in China was emitted from coal combustions (Xu et al., 2000). Additionally, in many cities of Shandong such as Jinan, nearly 40% of the gross domestic product was contributed by typical industries including coal-fired power plants (Cui et al., 2015). Therefore, regulations on improving combustion efficiency and constructing pollution control facilities in coal-fired power plants are necessary to lower $NO_3^-$ concentration.

Third, $NO_3^-$ was generally high over major city clusters (i.e., BTH, YRD, PRD, and CY) with a level of 10–15 $\mu g\,m^{-3}$ (Figure 4). This is related to the fact that vehicle populations of these regions grew exponentially, offsetting benefits from regulations on industry facilities and fuel quality (Fan et al., 2020). Although Beijing's License Lottery has been implemented since 2011 to limit the number of cars, the civilian vehicle population of Beijing has increased by 3.6 million from 2005–2018, as reported by the National Bureau of Statistics of China. In Chengdu and Chongqing where do not have central heating but vehicle usage is the highest among cities in China. In sparsely populated regions (i.e., Tibetan Plateau), $NO_3^-$ was lower than 3 $\mu g\,m^{-3}$ due to favorable weather conditions (i.e., strong wind) and scarce industrial activities.

Figure S4 compares the spatial distribution of seasonal averaged $NO_3^-$ during the study period. The highest $NO_3^-$ level was observed in winter mainly because China's central heating system is coal-burning based, making coal combustion the dominant source of $NO_3^-$ during the heating season (Zhao et al., 2020). Populous provinces in North China with central heating (i.e., Hebei, Henan, and Shandong) experienced high $NO_3^-$ at about 20 $\mu g\,m^{-3}$ (colored in dark red). In addition to anthropogenic factors, meteorological conditions such as low temperature raised $NO_3^-$ in winter. $NO_3^-$ of spring and autumn was similar, except $NO_3^-$ was higher in autumn over North China because central heating started in the region in late October or early November. The lowest $NO_3^-$ was observed in summer months with a concentration generally under 5 $\mu g\,m^{-3}$ (colored in blue) across China but increased to 8–10 $\mu g\,m^{-3}$ over provinces with many power plants and along traffic corridors, confirming again industrial and vehicle emissions make significant contributions to $NO_3^-$ pollution in China.
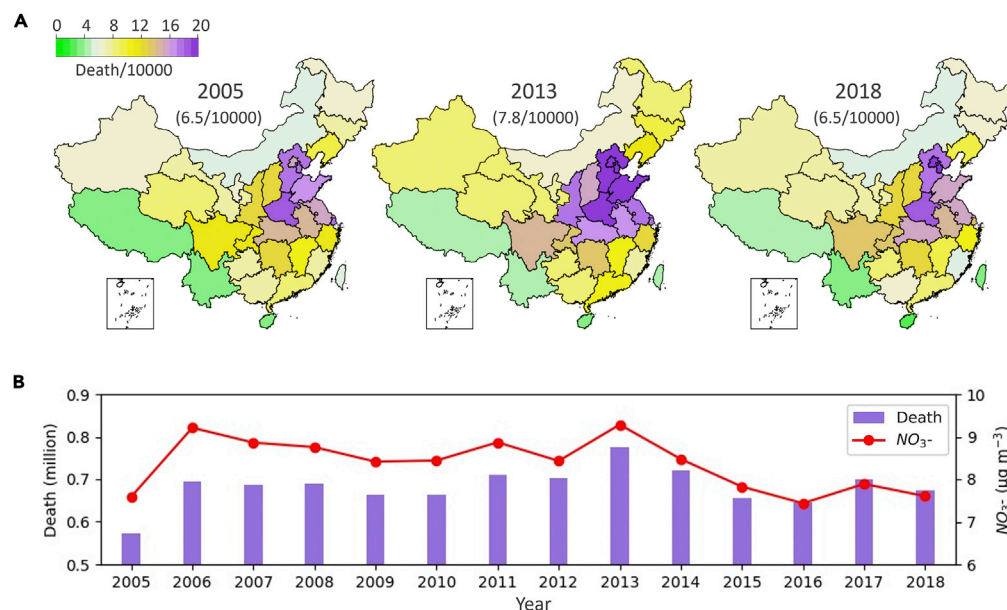
**Figure 5. Annual mean mortality burden of long-term NO₃- exposure in China.**

(A) compares the annual mean premature death rate of NO₃- (per 10,000 persons per year) in each province of China in 2005, 2013, and 2018. The color of the map refers to the upper left color bar. The national annual mean death rate for each year is shown in parentheses.

(B) shows the national mean annual NO₃- concentration (red dotted line, refers to the right y axis) and its corresponding premature death number (purple bars, refers to the left y axis) from 2005–2018.

### Mortality burden attributable to long-term $NO_3^-$ in China

The mortality burden of long-term $NO_3^-$ exposure in China has not been previously investigated though the burden of total $PM_{2.5}$ has been extensively studied. It is estimated that long-term $PM_{2.5}$ exposures accounted for an annual burden ranging from 1.5 to 2.2 million across the adult population in China (Liang et al., 2020). The heavy health burden exhibited strong spatial variations, with high attributable deaths concentrated in populated areas such as Beijing (Liu et al., 2017b), and developing inner provinces like He-bei because of the relocation of more polluting industries into these regions (Xie et al., 2016). However, none of these studies explored the long-term mortality burden from $NO_3^-$ due to the lack of a nationwide $NO_3^-$ exposure assessment. With the newly developed $NO_3^-$ model, for the first time, we estimated the mortality burden of long-term $NO_3^-$ exposure in China. We utilized a pooled relative risk (RR) reported by a meta-analysis (Yang et al., 2019) summarizing the health effect of $NO_3^-$ from three cohort studies, including estimates from Medicare Cohort, California Teachers Study conducted in the United States, and a cohort of 2.4 million people in Canada. For an interquartile range (IQR = 2.3 $\mu g\ m^{-3}$) increase in $NO_3^-$ level, the pooled RR increases by 2.6% (95% CI: 0.88%, 4.34%) (Yang et al., 2019).

Figure 5A displays the annual mean premature death rate (counts per 10,000 persons per year) attributed to $NO_3^-$ in each province of China in the first (2005) and last (2018) year of the study period and the year APPCAP was implemented (2013). During the study period, the highest death rate occurred in 2013 with a national annual mean of 7.8 per 10,000 persons. Regionally, the death rate of BTH, Henan, and Shandong was more than twice the national average, at about 20 per 10,000 persons. Low death rates were observed in Tibet, Yunnan, Hainan, and Taiwan where rates were below 5 per 10,000 persons. In 2018, the national mean death rate dropped back to 6.5 per 10,000 persons, equal to the death rate level in 2005. The reduction was mainly contributed by improved provincial death rates in Hebei, Henan, and Shandong where the rate decreased by nearly 50% after 2013. Comparing the death rate in 2018 with that in 2005, Beijing, Tianjin, Chongqing, and Sichuan were the only regions where the death rate increased by more than 1 per 10,000 persons. This reinforces that $NO_3^-$ regulations on coal-fired power plants were effective but need more effort to control vehicle emissions.

Figure 5B shows the national annual mean $NO_3^-$ concentration (red dotted line) and the total number of adult premature deaths attributable to the $NO_3^-$ exposure (purple bars) during the study period. Overall,

long-term $NO_3^-$ pollution brought 9.6 (95%, CI: 3.6–15.3) million deaths, accounting for about 1/3 of the death number caused by the total $PM_{2.5}$ pollution (Liang et al., 2020). Note that the national annual mean $NO_3^-$ concentration was around 8 μg m$^{-3}$, only accounted for up to 25% of $PM_{2.5}$ concentration (Liang et al., 2020), indicating $NO_3^-$ is of potential disproportionally high toxicity compared to the toxicity of total $PM_{2.5}$ (Ostro et al., 2015). During APPCAP, a reduction of 20.4% in the national mean $NO_3^-$ concentration was observed from 2013–2016, and correspondingly, the premature death number decreased from 0.77 (95%, CI: 0.28–1.23) million to 0.65 (95%, CI: 0.23–1.04) million. However, the death number increased to 0.68 (95%, CI: 0.24–1.08) million in 2018, confirming that China's clean air actions were successful but may need more effort to reduce $NO_3^-$ air pollution.

## Conclusion

In this study, we present a high-performance model to estimate long-term $NO_3^-$ concentration at 10-km resolution across China from 2005–2018, based on a random forest approach incorporating ground observations, satellite remote sensing data, model reanalysis, and other supporting information. Compared with a typical $PM_{2.5}$ mass prediction model, we included a unique set of variables tailored for $NO_3^-$ according to its physical characteristics and formation mechanisms. For example, MISR's AOD data were used to capture the spherical shape and high light reflectance of fine particles rich in $NO_3^-$. Unlike the previous studies with limited spatial coverage and model performance (Zhai et al., 2021; Geng et al., 2019), our model is able to provide spatially resolved high-quality predictions nationwide. The predicted long-term $NO_3^-$ trend can be applied to investigate the effectiveness of existing emission control policies and regulations relative to reducing $PM_{2.5}$ air pollution. Also, our model could help refine the health effect assessment of $NO_3^-$ such as we calculated the mortality burden of $NO_3^-$ in each province of China. Our findings indicate that relative to its mass fraction in $PM_{2.5}$, $NO_3^-$ might represent a greater population health risk in China. These estimates will greatly benefit epidemiological studies on accessing the health effect of $PM_{2.5}$ chemical compositions in China and other regions. The results presented here reinforce the need to better understand global excess mortality from ambient air pollution.

## Limitations of the study

Our $NO_3^-$ prediction model has a few limitations. First, the spatial and temporal characteristics of ground data used to train the random forest model might introduce sampling bias in the results. We included $NO_3^-$ observations from available 88 monitoring sites because China does not have a monitoring network of $PM_{2.5}$ constituents. Luckily, these monitoring sites have covered regions with different population densities and road lengths (Figure S5). In addition, 43 (49%) sites are located in rural areas and 45 (51%) sites are distributed in urban areas. However, most observations available before 2013 were collected from sites in Hong Kong and Taiwan because very few $PM_{2.5}$ speciation monitoring sites existed in mainland China. Regarding the discussion of city clusters, the different numbers of monitoring sites of different clusters will affect the spatial variation of $NO_3^-$ prediction (Figure S3B). In the future, we will include more ground observations when they are available to improve the model's stability and accuracy.

Second, although MISR provides unique information on aerosol microphysical properties, it has a narrow swath that leads to limited spatial coverage. As shown in Figures 4 and S4, $NO_3^-$ prediction was unavailable over eastern Tibet (colored in white). Gap-filling approaches are needed to fill missing AOD retrievals to improve the model's spatial coverage. Besides, MISR's low temporal resolution with global coverage of every nine days is limited to capturing the influence of non-fossil fuel $NO_x$ that contributes an important contribution to $NO_3^-$. Satellite observations with higher resolutions are needed to detect small burning spots in China and be added to the prediction model to verify the effect of biomass burning on $NO_3^-$ concentration.

Third, health risk estimates of long-term $NO_3^-$ exposure in China are not available at the time of this study. The pooled RR was calculated based on three cohort studies conducted either in the United States or Canada, where $NO_3^-$ concentration was much lower than the level in China. China's population susceptibility and socioeconomic characteristics were significantly different from these developed countries. As a result, the RR may be limited in fully representing the adverse health effect of $NO_3^-$ for the Chinese population. We will generate a nation-specific health risk assessment when a cohort study of $NO_3^-$ in China is available. In addition, only one-year data of age-specific baseline mortality was used in estimating mortality burdens due to the lack of data from other years during our study period. The National Bureau of Statistics of China (http://data.stats.gov.cn/) reported that the population of people 65 years or older increased by 66 million

from 2005 to 2018. Therefore, we may have underestimated the mortality burden of $NO_3^-$ in China of recent years because of the increasing population vulnerability to $NO_3^-$ pollution (Liang et al., 2020).

## STAR★METHODS

Detailed methods are provided in the online version of this paper and include the following:

- KEY RESOURCES TABLE
- RESOURCE AVAILABILITY
  - Lead contact
  - Materials availability
  - Data and code availability
- METHOD DETAILS
  - Observation of $NO_3^-$ concentration
  - Satellite-retrieved AOD
  - Other variables for model development
  - $NO_3^-$ model development
  - Estimation of the mortality burden of $NO_3^-$

## SUPPLEMENTAL INFORMATION

Supplemental information can be found online at https://doi.org/10.1016/j.isci.2022.104899.

## AUTHOR CONTRIBUTIONS

Y.H., X.M., and Y.L. designed the modeling procedure; Y.H., S.D., and Y.L. wrote the manuscript; Y.H. and X.M. conducted the data analysis with data provided by T.L., T.W., J.C., Q.F., S.L., K.H., F.L., H.K., and X.S.

## DECLARATION OF INTERESTS

The authors declare no competing interests.

## SUPPORTING CITATIONS

The following references appear in the supplemental information: Chen et al., 2018b; Deng et al., 2011; Gao et al., 2018; Huang et al., 2010; Li et al., 2015; State Council of the People's Republic of China, 2013; Wang et al., 2016.

## REFERENCES

Apte, J.S., Marshall, J.D., Cohen, A.J., and Brauer, M. (2015). Addressing global mortality from ambient PM2. 5. Environ. Sci. Technol. *49*, 8057–8066.

Breiman, L. (2001). Random forests. Mach. Learn. *45*, 5–32.

Burnett, R., Chen, H., Szyszkowicz, M., Fann, N., Hubbell, B., Pope, C.A., Apte, J.S., Brauer, M., Cohen, A., Weichenthal, S., et al. (2018). Global estimates of mortality associated with long-term exposure to outdoor fine particulate matter. Proc. Natl. Acad. Sci. USA *115*, 9592–9597.

Cao, J., Xu, H., Xu, Q., Chen, B., and Kan, H. (2012). Fine particulate matter constituents and cardiopulmonary mortality in a heavily polluted Chinese city. Environ. Health Perspect. *120*, 373–378.

Chang, Y., Zou, Z., Deng, C., Huang, K., Collett, J.L., Lin, J., and Zhuang, G. (2016). The importance of vehicle emissions as a source of atmospheric ammonia in the megacity of Shanghai. Atmos. Chem. Phys. *16*, 3577–3594.

Chau, K., Franklin, M., and Gauderman, W.J. (2020). Satellite-derived PM2. 5 composition and

its differential effect on children's lung function. Rem. Sens. *12*, 1028.

Chen, G., Li, S., Knibbs, L.D., Hamm, N.A.S., Cao, W., Li, T., Guo, J., Ren, H., Abramson, M.J., and Guo, Y. (2018a). A machine learning method to estimate PM2. 5 concentrations across China with remote sensing, meteorological and land use information. Sci. Total Environ. *636*, 52–60.

Chen, P., Wang, T., Kasoar, M., Xie, M., Li, S., Zhuang, B., and Li, M. (2018b). Source apportionment of PM2. 5 during haze and

non-haze episodes in Wuxi, China. Atmosphere 9, 267.

Chen, Y., Jin, G.Z., Kumar, N., and Shi, G. (2013). The promise of Beijing: evaluating the impact of the 2008 Olympic Games on air quality. J. Environ. Econ. Manag. 66, 424–443.

Chung, Y., Dominici, F., Wang, Y., Coull, B.A., and Bell, M.L. (2015). Associations between long-term exposure to chemical constituents of fine particulate matter (PM2. 5) and mortality in Medicare enrollees in the eastern United States. Environ. Health Perspect. 123, 467–474.

Cohen, A.J., Brauer, M., Burnett, R., Anderson, H.R., Frostad, J., Estep, K., Balakrishnan, K., Brunekreef, B., Dandona, L., Dandona, R., et al. (2017). Estimates and 25-year trends of the global burden of disease attributable to ambient air pollution: an analysis of data from the Global Burden of Diseases Study 2015. Lancet 389, 1907–1918.

Cui, L.L., Zhang, J., Zhou, J., Zhang, Y., and Li, T. (2015). Acute respiratory and cardiovascular health effects of an air pollution event, January 2013, Jinan, China. Publ. Health 131, 99–102.

Deng, C., Zhuang, G., Huang, K., Li, J., Zhang, R., Wang, Q., Liu, T., Sun, Y., Guo, Z., and Fu, J.S. (2011). Chemical characterization of aerosols at the summit of mountain Tai in central East China. Atmos. Chem. Phys. 11, 7319–7332.

Diner, D.J., Beckert, J.C., Reilly, T.H., Bruegge, C.J., Conel, J.E., Kahn, R.A., Martonchik, J.V., Ackerman, T.P., Davies, R., Gerstl, S., et al. (1998). Multi-angle Imaging SpectroRadiometer (MISR) instrument description and experiment overview. IEEE Trans. Geosci. Remote Sens. 36, 1072–1087.

Dong, H.-B., Zeng, L.-M., Hu, M., Wu, Y.-S., Zhang, Y.-H., Slanina, J., Zheng, M., Wang, Z.-F., and JANSEN, R. (2012). The application of an improved gas and aerosol collector for ambient air pollutants in China. Atmos. Chem. Phys. 12, 10519–10533.

Fan, M., Zhang, Y., Lin, Y., Cao, F., Zhao, Z., Sun, Y., Qiu, Y., Fu, P., and Wang, Y. (2020). Changes of emission sources to nitrate aerosols in Beijing after the clean air actions: evidence from dual isotope compositions. J. Geophys. Res. Atmos. 125. e2019JD031998.

Feng, T., Bei, N., Zhao, S., Wu, J., Liu, S., Li, X., Liu, L., Wang, R., Zhang, X., Tie, X., and Li, G. (2021). Nitrate debuts as a dominant contributor to particulate pollution in Beijing: roles of enhanced atmospheric oxidizing capacity and decreased sulfur dioxide emission. Atmos. Environ. 244, 117995.

Franklin, M., Kalashnikova, O.V., and Garay, M.J. (2017). Size-resolved particulate matter concentrations derived from 4.4 km-resolution size-fractionated Multi-angle Imaging SpectroRadiometer (MISR) aerosol optical depth over Southern California. Rem. Sens. Environ. 196, 312–323.

Friberg, M.D., Zhai, X., Holmes, H.A., Chang, H.H., Strickland, M.J., Sarnat, S.E., Tolbert, P.E., Russell, A.G., and Mulholland, J.A. (2016). Method for fusing observational data and chemical transport model simulations to estimate spatiotemporally resolved ambient air pollution. Environ. Sci. Technol. 50, 3695–3705.

Garay, M.J., Witek, M.L., Kahn, R.A., Seidel, F.C., Limbacher, J.A., Bull, M.A., Diner, D.J., Hansen, E.G., Kalashnikova, O.V., LEE, H., et al. (2020). Introducing the 4.4 km spatial resolution Multi-Angle Imaging SpectroRadiometer (MISR) aerosol product. Atmos. Meas. Tech. 13, 593–628.

Gao, J., Wang, K., Wang, Y., Liu, S., Zhu, C., Hao, J., Liu, H., Hua, S., and Tian, H. (2018). Temporal-spatial characteristics and source apportionment of PM2. 5 as well as its associated chemical species in the Beijing-Tianjin-Hebei region of China. Environ. Pollut. 233, 714–724.

Geng, G., Meng, X., He, K., and Liu, Y. (2020). Random forest models for PM2. 5 speciation concentrations using MISR fractional AODs. Environ. Res. Lett. 15, 034056.

Geng, G., Xiao, Q., Zheng, Y., Tong, D., Zhang, Y., Zhang, X., Zhang, Q., He, K., and Liu, Y. (2019). Impact of China's air pollution prevention and control action plan on PM 2.5 chemical composition over eastern China. Sci. China Earth Sci. 62, 1872–1884.

Geng, G., Zhang, Q., Tong, D., Li, M., Zheng, Y., Wang, S., and He, K. (2017). Chemical composition of ambient PM 2. 5 over China and relationship to precursor emissions during 2005–2012. Atmos. Chem. Phys. 17, 9187–9203.

Hu, X., Belle, J.H., Meng, X., Wildani, A., Waller, L.A., Strickland, M.J., and Liu, Y. (2017). Estimating PM2.5 concentrations in the conterminous United States using the random forest approach. Environ. Sci. Technol. 51, 6936–6944.

Huang, X.H., Bian, Q., Ng, W.M., Louie, P.K., and Yu, J.Z. (2014). Characterization of PM2. 5 major components and source investigation in suburban Hong Kong: a one year monitoring study. Aerosol Air Qual. Res. 14, 237–250.

Huang, K., Zhuang, G., Li, J., Wang, Q., Sun, Y., Lin, Y., and Fu, J.S. (2010). Mixing of Asian dust with pollution aerosol and the transformation of aerosol components during the dust storm over China in spring 2007. J. Geophys. Res. 115, D00K13.

Inness, A., Ades, M., Agustí-Panareda, A., Barré, J., Benedictow, A., Blechschmidt, A.-M., Dominguez, J.J., Engelen, R., Eskes, H., Flemming, J., et al. (2019). The CAMS reanalysis of atmospheric composition. Atmos. Chem. Phys. 19, 3515–3556.

Jin, Y., Andersson, H., and Zhang, S. (2016). Air pollution control policies in China: a retrospective and prospects. Int. J. Environ. Res. Public Health 13, 1219.

Kahn, R.A., Gaitley, B.J., Martonchik, J.V., Diner, D.J., Crean, K.A., and Holben, B. (2005). Multiangle Imaging Spectroradiometer (MISR) global aerosol optical depth validation based on 2 years of coincident Aerosol Robotic Network (AERONET) observations. J. Geophys. Res. 110, D10S04.

Kong, L., Feng, M., Liu, Y., Zhang, Y., Zhang, C., Li, C., Qu, Y., An, J., Liu, X., Tan, Q., et al. (2020). Elucidating the pollution characteristics of nitrate, sulfate and ammonium in PM 2.5 in Chengdu, southwest China, based on 3-year measurements. Atmos. Chem. Phys. 20, 11181–11199.

Li, M., Liu, H., Geng, G., Hong, C., Liu, F., Song, Y., Tong, D., Zheng, B., Cui, H., Man, H., et al. (2017). Anthropogenic emission inventories in China: a review. Natl. Sci. Rev. 4, 834–866.

Li, P., Xin, J., Wang, Y., Li, G., Pan, X., Wang, S., Cheng, M., Wen, T., Wang, G., and Liu, Z. (2015). Association between particulate matter and its chemical constituents of urban air pollution and daily mortality or morbidity in Beijing City. Environ. Sci. Pollut. Res. 22, 358–368.

Li, R., Cui, L., Zhao, Y., Zhou, W., and Fu, H. (2021). Long-term trends of ambient nitrate (NO 3—) concentrations across China based on ensemble machine-learning models. Earth Syst. Sci. Data 13, 2147–2163.

Liang, F., Xiao, Q., Huang, K., Yang, X., Liu, F., Li, J., Lu, X., Liu, Y., and Gu, D. (2020). The 17-y spatiotemporal trend of PM2. 5 and its mortality burden in China. Proc. Natl. Acad. Sci. USA 117, 25601–25608.

Lin, C.-H., Wu, Y.-L., Lai, C.-H., Watson, J.G., and Chow, J.C. (2008). Air quality measurements from the southern particulate matter supersite in Taiwan. Aerosol Air Qual. Res. 8, 233–264.

Lin, H., Tao, J., Du, Y., Liu, T., Qian, Z., Tian, L., Di, Q., Rutherford, S., Guo, L., Zeng, W., et al. (2016). Particle size and chemical constituents of ambient particulate pollution associated with cardiovascular mortality in Guangzhou, China. Environ. Pollut. 208, 758–766.

Liu, L., Zhang, X., Zhang, Y., Xu, W., Liu, X., Zhang, X., Feng, J., Chen, X., Zhang, Y., Lu, X., et al. (2017a). Dry particulate nitrate deposition in China. Environ. Sci. Technol. 51, 5572–5581.

Liu, M., Huang, X., Song, Y., Xu, T., Wang, S., Wu, Z., Hu, M., Zhang, L., Zhang, Q., Pan, Y., et al. (2018). Rapid SO 2 emission reductions significantly increase tropospheric ammonia concentrations over the North China Plain. Atmos. Chem. Phys. 18, 17933–17943.

Liu, M., Huang, Y., Ma, Z., Jin, Z., Liu, X., Wang, H., Liu, Y., Wang, J., Jantunen, M., Bi, J., and Kinney, P.L. (2017b). Spatial and temporal trends in the mortality burden of air pollution in China: 2004–2012. Environ. Int. 98, 75–81.

Liu, S., and Zhang, K. (2015). Fine particulate matter components and mortality in Greater Houston: did the risk reduce from 2000 to 2011? Sci. Total Environ. 538, 162–168.

Liu, X., Zhang, Y., Cheng, Y., Hu, M., and Han, T. (2012). Aerosol hygroscopicity and its impact on atmospheric visibility and radiative forcing in Guangzhou during the 2006 PRIDE-PRD campaign. Atmos. Environ. 60, 59–67.

Liu, X., Zhang, Y., Han, W., Tang, A., Shen, J., Cui, Z., Vitousek, P., Erisman, J.W., Goulding, K., Christie, P., et al. (2013). Enhanced nitrogen deposition over China. Nature 494, 459–462.

Liu, Y., Koutrakis, P., and Kahn, R. (2007). Estimating fine particulate matter component concentrations and size distributions using satellite-retrieved fractional aerosol optical depth: Part 1—method development. J. Air Waste Manag. Assoc. 57, 1351–1359.

Meng, X., Garay, M.J., Diner, D.J., Kalashnikova, O.V., Xu, J., and Liu, Y. (2018a). Estimating PM2. 5

speciation concentrations using prototype 4.4 km-resolution MISR aerosol properties over Southern California. Atmos. Environ. *181*, 70–81.

Meng, X., Hand, J.L., Schichtel, B.A., and Liu, Y. (2018b). Space-time trends of PM2. 5 constituents in the conterminous United States estimated by a machine learning approach, 2005–2015. Environ. Int. *121*, 1137–1147.

Ostro, B., Hu, J., Goldberg, D., Reynolds, P., Hertz, A., Bernstein, L., and Kleeman, M.J. (2015). Associations of mortality with long-term exposures to fine and ultrafine particles, species and sources: results from the California Teachers Study Cohort. Environ. Health Perspect. *123*, 549–556.

Ostro, B., Roth, L., Malig, B., and Marty, M. (2009). The effects of fine particle components on respiratory hospital admissions in children. Environ. Health Perspect. *117*, 475–480.

Park, M., Joo, H.S., Lee, K., Jang, M., Kim, S.D., Kim, I., Borlaza, L.J.S., Lim, H., Shin, H., Chung, K.H., et al. (2018). Differential toxicities of fine particulate matters from various sources. Sci. Rep. *8*, 17007.

Peng, R.D., Bell, M.L., Geyh, A.S., Mcdermott, A., Zeger, S.L., Samet, J.M., and Dominici, F. (2009). Emergency admissions for cardiovascular and respiratory diseases and the chemical composition of fine particle air pollution. Environ. Health Perspect. *117*, 957–963.

Shao, P., Tian, H., Sun, Y., Liu, H., Wu, B., Liu, S., Liu, X., Wu, Y., Liang, W., Wang, Y., et al. (2018). Characterizing remarkable changes of severe haze events and chemical compositions in multi-size airborne particles (PM1, PM2.5 and PM10 ) from January 2013 to 2016-2017 winter in Beijing, China. Atmos. Environ. *189*, 133–144.

Shen, F., Zhang, L., Jiang, L., Tang, M., Gai, X., Chen, M., and Ge, X. (2020). Temporal variations of six ambient criteria air pollutants from 2015 to 2018, their spatial distributions, health risks and relationships with socioeconomic factors during 2018 in China. Environ. Int. *137*, 105556.

Son, J.-Y., Lee, J.-T., Kim, K.-H., Jung, K., and Bell, M.L. (2012). Characterization of fine particulate matter and associations between particulate chemical constituents and mortality in Seoul, Korea. Environ. Health Perspect. *120*, 872–878.

State Council of the People's Republic of China (2013). Air Pollution Prevention and Control Action Plan (State Council of the People's Republic of China).

Stelson, A.W., Bassett, M.E., and Seinfeld, J.H. (1984). Thermodynamic Equilibrium Properties of Aqueous Solutions of Nitrate, Sulfate and Ammonium. In Chemistry of particles, fogs, and rain. Acid precipitation series. No.2 (Butterworth Publishers), pp. 1–52. ISBN 9780250405671.

Sun, K., Tao, L., Miller, D.J., Pan, D., Golston, L.M., Zondlo, M.A., Griffin, R.J., Wallace, H.W., Leong, Y.J., Yang, M.M., et al. (2017). Vehicle emissions as an important urban ammonia source in the United States and China. Environ. Sci. Technol. *51*, 2472–2481.

Turap, Y., Talifu, D., Wang, X., Abulizi, A., Maihemuti, M., Tursun, Y., Ding, X., Aierken, T., and Rekefu, S. (2019). Temporal distribution and source apportionment of PM2.5 chemical composition in Xinjiang, NW-China. Atmos. Res. *218*, 257–268.

van der A, R.J., Mijling, B., Ding, J., Koukouli, M.E., Liu, F., Li, Q., Mao, H., and Theys, N. (2017). Cleaning up the air: effectiveness of air quality policy for SO 2 and NO x emissions in China. Atmos. Chem. Phys. *17*, 1775–1789.

WHO (2007). Health Relevance of Particulate Matter from Various Sources: Report on a WHO Workshop (Bonn, Germany: World Health Organization).

Wang, D., Zhou, B., Fu, Q., Zhao, Q., Zhang, Q., Chen, J., Yang, X., Duan, Y., and Li, J. (2016). Intense secondary aerosol formation due to strong atmospheric photochemical reactions in summer: observations at a rural site in eastern Yangtze River Delta of China. Sci. Total Environ. *571*, 1454–1466.

Wu, Y., Gu, B., Erisman, J.W., Reis, S., Fang, Y., Lu, X., and Zhang, X. (2016). PM2. 5 pollution is substantially affected by ammonia emissions in China. Environ. Pollut. *218*, 86–94.

Wu, Y., Zhang, S., Hao, J., Liu, H., Wu, X., Hu, J., Walsh, M.P., Wallington, T.J., Zhang, K.M., and Stevanovic, S. (2017). On-road vehicle emissions and their control in China: a review and outlook. Sci. Total Environ. *574*, 332–349.

Xiao, Q., Chang, H.H., Geng, G., and Liu, Y. (2018). An ensemble machine-learning model to predict historical PM2. 5 concentrations in China from satellite data. Environ. Sci. Technol. *52*, 13260–13269.

Xie, R., Sabel, C.E., Lu, X., Zhu, W., Kan, H., Nielsen, C.P., and Wang, H. (2016). Long-term trend and spatial pattern of PM2. 5 induced premature mortality in China. Environ. Int. *97*, 180–186.

Xing, J., Mathur, R., Pleim, J., Hogrefe, C., Gan, C.-M., Wong, D.-C., Wei, C., Gilliam, R., and Pouliot, G. (2015). Observations and modeling of air quality trends over 1990–2010 across the Northern Hemisphere: China, the United States and Europe. Atmos. Chem. Phys. *15*, 2723–2747.

Xu, Q., Wang, S., Jiang, J., Bhattarai, N., Li, X., Chang, X., Qiu, X., Zheng, M., Hua, Y., and Hao, J. (2019). Nitrate dominates the chemical composition of PM2.5 during haze event in Beijing, China. Sci. Total Environ. *689*, 1293–1303.

Xu, X., Chen, C., Qi, H., He, R., You, C., and Xiang, G. (2000). Development of coal combustion pollution control for SO2 and NOx in China. Fuel Process. Technol. *62*, 153–160.

Yang, Y., Ruan, Z., Wang, X., Yang, Y., Mason, T.G., Lin, H., and Tian, L. (2019). Short-term and long-term exposures to fine particulate matter constituents and health: a systematic review and meta-analysis. Environ. Pollut. *247*, 874–882.

Zhai, S., Jacob, D.J., Wang, X., Liu, Z., Wen, T., Shah, V., Li, K., Moch, J.M., Bates, K.H., Song, S., et al. (2021). Control of particulate nitrate air pollution in China. Nat. Geosci. *14*, 389–395.

Zhang, L., Chen, Y., Zhao, Y., Henze, D.K., Zhu, L., Song, Y., Paulot, F., Liu, X., Pan, Y., Lin, Y., and Huang, B. (2018). Agricultural ammonia emissions in China: reconciling bottom-up and top-down estimates. Atmos. Chem. Phys. *18*, 339–355.

Zhang, Q., Zheng, Y., Tong, D., Shao, M., Wang, S., Zhang, Y., Xu, X., Wang, J., He, H., Liu, W., et al. (2019a). Drivers of improved PM2. 5 air quality in China from 2013 to 2017. Proc. Natl. Acad. Sci. USA *116*, 24463–24469.

Zhang, X., Xu, X., Ding, Y., Liu, Y., Zhang, H., Wang, Y., and Zhong, J. (2019b). The impact of meteorological changes from 2013 to 2017 on PM 2.5 mass reduction in key regions in China. Sci. China Earth Sci. *62*, 1885–1902.

Zhao, B., Wang, P., Ma, J.Z., Zhu, S., Pozzer, A., and Li, W. (2012). A high-resolution emission inventory of primary pollutants for the Huabei region, China. Atmos. Chem. Phys. *12*, 481–501.

Zhao, C., Niu, M., Song, S., Li, J., Su, Z., Wang, Y., Gao, Q., and Wang, H. (2019). Serum metabolomics analysis of mice that received repeated airway exposure to a water-soluble PM2. 5 extract. Ecotoxicol. Environ. Saf. *168*, 102–109.

Zhao, Y., Xi, M., Zhang, Q., Dong, Z., Ma, M., Zhou, K., Xu, W., Xing, J., Zheng, B., Wen, Z., et al. (2022). Decline in bulk deposition of air pollutants in China lags behind reductions in emissions. Nat. Geosci. *15*, 190–195.

Zhao, Z.-Y., Cao, F., Fan, M.-Y., Zhang, W.-Q., Zhai, X.-Y., Wang, Q., and Zhang, Y.-L. (2020). Coal and biomass burning as major emissions of NOX in Northeast China: implication from dual isotopes analysis of fine nitrate aerosols. Atmos. Environ. *242*, 117762.

Zheng, B., Tong, D., Li, M., Liu, F., Hong, C., Geng, G., Li, H., Li, X., Peng, L., Qi, J., et al. (2018). Trends in China's anthropogenic emissions since 2010 as the consequence of clean air actions. Atmos. Chem. Phys. *18*, 14095–14111.

Zhong, Q., Tao, S., Ma, J., Liu, J., Shen, H., Shen, G., Guan, D., Yun, X., Meng, W., Yu, X., et al. (2021). PM2. 5 reductions in Chinese cities from 2013 to 2019 remain significant despite the inflating effects of meteorological conditions. One Earth *4*, 448–458.

Zhou, W., Gao, M., He, Y., Wang, Q., Xie, C., Xu, W., Zhao, J., Du, W., Qiu, Y., Lei, L., et al. (2019). Response of aerosol chemistry to clean air action in Beijing, China: insights from two-year ACSM measurements and model simulations. Environ. Pollut. *255*, 113345.

# STAR★METHODS

## KEY RESOURCES TABLE

| REAGENT or RESOURCE | SOURCE | IDENTIFIER |
|---|---|---|
| Software and algorithms | | |
| Python 3.8.8 | Python Software Foundation | https://www.python.org/ |

## RESOURCE AVAILABILITY

### Lead contact

Further information and requests for resources should be directed to and will be fulfilled by the lead contact, Yang Liu (yang.liu@emory.edu).

### Materials availability

This study did not generate new unique materials.

### Data and code availability

- Relevant data sources for modeling are provided in the paper and supplemental information.

- Codes for the maps of this study are available from the corresponding authors on reasonable request.

- Any additional information required to reanalyze the data reported in this paper is available from the lead contact upon request.

## METHOD DETAILS

### Observation of $NO_3^-$ concentration

We collected approximately 21,000 ground observational records of daily mean $NO_3^-$ concentration from 88 monitoring sites, as listed in Table S1. High-quality $NO_3^-$ data from Hong Kong and Taiwan $PM_{2.5}$ speciation supersites were also included (Lin et al., 2008; Huang et al., 2014). According to the Finer Resolution Observation and Monitoring Global Land Cover data (http://data.ess.tsinghua.edu.cn/) that provides information on area type, 43 of the 88 (49%) monitoring sites are located in rural areas. Histograms of population density and road length of monitoring sites (Figure S5) show that the ground data has covered regions with different population density and road length levels. Both filter-based and online-based methods are used in these sites to measure $NO_3^-$ as China does not have a $PM_{2.5}$ species monitoring network with uniform standards. Previous research reported that $NO_3^-$ concentration measured by filter method is highly consistent with measurements from the online method in China (Dong et al., 2012), so we used all the available $NO_3^-$ observations from 2005–2018 to ensure sufficient model training.

### Satellite-retrieved AOD

MISR aboard satellite Terra was launched in 1999 to measure upwelling solar radiance in four spectral bands (0.446 μm, 0.558 μm, 0.672 μm, and 0.866 μm) and at nine view angles ($0°$, $\pm 26.1°$, $\pm 45.6°$, $\pm 60°$, $\pm 70.5°$) over a 360 km swath (Diner et al., 1998). This wide range of along-track view angles help the sensor accurately evaluate the surface contribution to the top-of-atmosphere radiances. MISR hence can provide globally continuous retrievals of AOD and information on aerosol microphysical properties over complex land surfaces (Kahn et al., 2005). Our study used the latest Version 23 MISR Level 2 aerosol product (Garay et al., 2020) to distinguish $NO_3^-$ above bright surfaces with an improved spatial resolution of $4.4 \times 4.4\text{-km}^2$. This stable and continuous satellite data make the prediction model reliable over regions where ground measurements are unavailable.

The MISR aerosol product supplies a set of aerosol mixtures that can be used to calculate eight types of aerosol components (#1, #2, #3, #6, #8, #14, #19, #21) based on aerosol's shape, size distribution, reflection property, and scale height. Detailed information about each aerosol component can be found in Liu et al. (2007). These aerosol components can be used to estimate different AOD types relating to the physical features of $NO_3^-$. For example, non-spherical AOD components (i.e., #19) and non-absorption AOD components (i.e., #2, #3, #6) were used in this study as predictors of $NO_3^-$. AOD values of small (particle radius

<0.35 μm) and large mode (particle radius >0.7 μm) particles provided by the MISR aerosol product were added to the model to reflect the bimodal distribution of $NO_3^-$. Since MISR only has a global coverage of 9 days at the equator and 2 days at the poles due to its relatively narrow swath, we used annual mean AOD data from 2005–2018 to develop the $NO_3^-$ model. We found that MISR AOD data can substantially improve the model's performance even though the data's temporal resolution is not high. As our study focus is annual mean $NO_3^-$ concentration, the temporal resolution of MISR AOD data will not influence our results. All AOD data presented here were processed at the grid cell level of 10-km.

### Other variables for model development

Atmospheric composition data of $PM_{2.5}$ at 10-km spatial resolution is adopted from a published study (Xiao et al., 2018). $NO_3^-$, NO, $NO_2$, and $HNO_3$ at $0.75 \times 0.75°$ spatial resolution with a 3-hourly temporal resolution during 2005–2018 were extracted from the latest global reanalysis dataset of atmospheric composition, Copernicus Atmosphere Monitoring Service (CAMS) reanalysis (Inness et al., 2019), produced by the European Centre for Medium-Range Weather Forecasts (ECMWF). This dataset shows smaller biases than other reanalysis data when comparing data quality with observations (Inness et al., 2019). All CAMS data used in our study were matched to 10-km grid cells at the daily level by the inverse distance weighting (IDW) method. Emission inventory of $NH_3$ also comes from CAMS but at monthly temporal resolution.

Meteorological variables including temperature at 2-meter, humidity at 2-meter, and planetary boundary layer height during 2005–2018 were derived from the Goddard Earth Observing System Model Forward Processing (GEOS-FP) product, which is able to produce real-time meteorological conditions using the most recent validated GEOS system with a spatial resolution of $0.25 \times 0.3125°$ ($0.5 \times 0.625°$ before 2013) and a temporal resolution of 3 hours (Apte et al., 2015). Similar to processing atmospheric composition data, all GEOS-FP data were interpolated to 10-km grid cells at the daily level.

Road networks of highway and city expressways in China were obtained from the Institute of Geographic Sciences and Natural Resources Research of the Chinese Academy of Sciences. Only 2014 data was applied to locate road position and length in our random forest model since it has the best data quality. NDVI data from 2005–2018 was extracted from Terra MODIS C6 monthly NDVI product (MOD13A3) at 1 km resolution to define different types of land surfaces.

### $NO_3^-$ model development

A $10 \times 10\text{-km}^2$ grid was designed to cover the entire study domain for model development. A total of 100,699 grid cells were within the border of the domain. We calculated the daily mean $NO_3^-$ concentration in each grid cell during 2005–2018 based on a random forest algorithm trained by available ground observations (Breiman, 2001), a process to build multiple decision trees and merge them to get an accurate and stable prediction of $NO_3^-$. A final prediction model is determined by comparing the result of different settings of predictors used to split tree nodes and the number of trees in the forest (Hu et al., 2017). This modeling method has been widely used and shows high predictive abilities to estimate historical air pollution (Chen et al., 2018a; Hu et al., 2017; Geng et al., 2020; Xiao et al., 2018). In this study, the $NO_3^-$ model was constructed by testing different predictors that can improve model performance (i.e., minimize mean squared error) and relate to $NO_3^-$ formation or spatial distribution. For example, we choose MISR AODs as predictors because they greatly improve the model performance in predicting $NO_3^-$ in West China. We select 18 predictors in the final model, including satellite-retrieved AODs and NDVI, model reanalysis of atmospheric composition and meteorological conditions, emission inventory, and road length to achieve the best prediction accuracy. We build 1000 trees in the prediction model to minimize the model's overfitting problem (Hu et al., 2017). Information on model variables and their permutation feature importance ranking is provided in Figure S2. Modeling data of $NO_3^-$, $PM_{2.5}$, $NO_2$, humidity and observational data of MISR AOD #19 ranked the top five significant predictors.

### Estimation of the mortality burden of $NO_3^-$

Mortality burden attributable to long-term $NO_3^-$ exposure was calculated based on $NO_3^-$ concentration, a meta-analysis pooled $NO_3^-$ RR (Yang et al., 2019), population size, and baseline mortality rate, following methods described in the Global Burden of Disease project (Apte et al., 2015) and Liang et al. (2020). All data presented here were linked to 10-km grid cells, then aggregated to the provincial level. To quantify the mortality risk of $NO_3^-$ pollution in China, the relative risk (RR) over each grid cell $i$ in year $j$, is defined as:

$$RR_{ij} = e^{\beta(x_{ij} - x_{cf})} \qquad \text{(Equation 1)}$$

where $\beta$ is the health effect of long-term $NO_3^-$ exposure, equal to 0.011 (95%, CI: 0.003-0.018), calculated based on pooled RR from a systematic review (Yang et al., 2019). Detailed information on $NO_3^-$ mortality RR estimates and associated interquartile range can be found in Yang et al. (2019) $x_{ij}$ represents the $NO_3^-$ concentration of each grid cell $i$ in year $j$, and $x_{cf}$ is the lowest $NO_3^-$ concentration estimated during the entire study period representing counterfactual exposure level. The population attributable fraction (*PAF*) of each grid cell $i$ in year $j$ is determined by:

$$PAF_{ij} = (RR_{ij} - 1)/RR_{ij} \qquad \text{(Equation 2)}$$

Then, the *PAF* of each province was derived using LandScan annual population data (https://landscan.ornl.gov/). Lastly, the annual absolute number of adult death counts attributable to $NO_3^-$ exposure at the provincial level is calculated using:

$$Mortality_{jk} = PAF_{jk} \times POP_{jk} \times I_{jk} \qquad \text{(Equation 3)}$$

*Mortality$_{jk}$* is the estimated premature deaths in province $k$ in year $j$; *PAF$_{jk}$* is the population attributable fraction; *POP$_{jk}$* and *I$_{jk}$* correspond to the total adult population ($\geq$25-year old) and the baseline mortality rate of adults, respectively. Annual age-specific population and all-cause mortality rate data were obtained from the National Bureau of Statistics of China (http://data.stats.gov.cn/), China Population and Employment Statistics Yearbooks, Census and Statistics Department of the Hong Kong (https://www.censtatd.gov.hk/), Macao (https://www.dsec.gov.mo/), Taiwan (https://www.stat.gov.tw/). Age-specific mortality data were obtained from demographic census statistics (http://data.stats.gov.cn/).